Available online at www.sciencedirect.com
SCIENCE DIRECT®
ELSEVIER
Journal of Magnetism and Magnetic Materials 257 (2003) 258–269
journal of magnetism and magnetic materials
www.elsevier.com/locate/jmmm

Texture and magneto-crystalline anisotropy analysis of an oriented $ErMn_4Fe_8C$ powder sample

M. Morales[a,*], D. Chateigner[b], D. Fruchart[c]

[a] Laboratoire d'Etude et de Recherche sur les Matériaux, ISMRA, 6 Boulevard Maréchal Juin, 14050 Caen Cedex, France
[b] Laboratoire de Cristallographie et Sciences des Matériaux, ISMRA, 6 Boulevard Maréchal Juin, 14050 Caen Cedex, France
[c] Laboratoire de Cristallographie, CNRS, BP166, 38042 Grenoble Cedex 09, France

Received 28 February 2002; received in revised form 4 September 2002

Abstract

Powder samples of the ternary carbide $ErMn_4Fe_8C_{x-1}$ were oriented under a low magnetic field $H \sim 0.5$ T. Analysis of the crystal texture of the samples confirms that the compound is of easy-plane type, in agreement with magnetization measurements and neutron diffraction experiments performed elsewhere. Both the latter techniques have revealed that the magnetic arrangement is rather complicated, as supported by competing contributions to magneto-crystalline anisotropy. However, assuming a reasonably simple expression for the magneto-crystalline anisotropy valid at high temperature only, the texture analysis, performed at 300 K, has allowed simulation of the magnetization versus field curve for this planar ferrimagnetic structure. A comparison with the experimental magnetization curve reveals the onset of a first-order magnetization process taking place under an applied field up to 1.8 T.

PACS: 75.30.Gw; 71.20.Lp; 61.10.Yh; 75.60.−d

Keywords: 4f–3d Intermetallics; Interstitial compounds; X-ray quantitative texture analysis; Magnetic anisotropy; Magnetization curves

1. Introduction

Most of the iron-rich intermetallic compounds of rare-earth elements (R) and 3d transition metals (M) are characterized by the existence of interstitial sites suited for the insertion of elements such as H, C or N. Thanks to the insertion of light elements in compounds having the $ThMn_{12}$ structure type, most of their fundamental characteristics, such as the 3d magnetization, the Curie temperature T_C and the magneto-crystalline anisotropy, are modified [1]. Previous studies on the insertion of H and C atoms in the $ErMn_{12-x}Fe_x$ compounds ($x \leqslant 9$) have revealed large modifications of the magnetic properties induced by the interstitial atoms; firstly a marked increase of T_C (e.g. $ErMn_4Fe_8C_{x-1}$, $\Delta T_C/T_C = 85\%$) and secondly a drastic change from easy-axis to easy-plane behavior with the insertion of C [2,3].

In order to optimize extrinsic anisotropic properties, a lot of effort has been devoted in the last decade to the development of texturing

*Corresponding author. Tel.: +33-2-31-45-25-02; fax: +33-2-31-45-26-60.
E-mail address: magali.morales@ismra.fr (M. Morales).

0304-8853/03/$ - see front matter
PII: S0304-8853(02)01207-6

processes. As the ability for magnetic moments to be aligned along the main crystal axis (easy-axis materials) is of fundamental importance for hard magnetic properties, many studies have been devoted to the characterization of the magneto-crystalline anisotropy via magnetization curves, e.g. in intermetallic compounds [4,5]. These analyses generally concentrate on the estimation of the crystallite distribution and the intrinsic magnetic properties (crystalline anisotropy constants K_1, K_2, sample polarization, etc.) from the magnetization curves, using differently defined orientation or misalignment parameters in easy-axis ferromagnetic compounds [4,5]. Since many parameters influence the magnetization curves, it seems relevant to measure them independently as much as possible. Besides, such orientation distribution factors are accessible for any crystalline material using diffraction measurements, and can be estimated using quantitative texture analysis (QTA) [6,7].

The aim of this paper is to simulate at $T = 300$ K the magnetization curve of the oriented easy-plane ferrimagnetic $ErMn_4Fe_8C$ sample [2,8] using the texture parameters (degree of orientation of the sample) determined by X-ray QTA analysis and assuming a reasonably simple expression for the magneto-crystalline anisotropy at high temperature.

2. Experimental

The starting compound $ErMn_4Fe_8$ was prepared by induction melting of the metal constituents in a water-cooled copper crucible under a purified argon atmosphere. For the synthesis of the ferrimagnetic $ErMn_4Fe_8C$ carbide, finely crushed powder of the starting compound was mixed with an excess amount of anthracene (by 10%) [8]. The mixed powders compacted into pellets, were sealed under vacuum in quartz tubes and annealed at $T = 623-673$ K during 4 days. Above 623 K, the anthracene decomposition provides elemental carbon, making possible the formation of ternary carbides [9]. A home-made thermomagnetic torque was used to determine the change in T_C upon carburation from 200 to 370 K, respectively, for the starting compound and the carbon charged compound [8]. In order to determine the macroscopic easy magnetization direction (EMD) and to estimate the magnetic anisotropy, two differently aligned samples were prepared by polymerization of a resin-powder mixture under an applied magnetic field, H_{text}, of 0.5 T. Both samples were 4 mm diameter and 5 mm long cylinders. Sample A was solidified with H_{text} applied parallel to the z-axis of the cylinder (Fig. 1, right column), while Sample B was rotated (10 rd/min) around its z-axis during polymerization [10] with H_{text} applied perpendicular to it (Fig. 1, left column).

Room temperature X-ray diffraction patterns were recorded in the Bragg–Brentano geometry (θ–2θ scans) on the two samples, with the scattering vector **S(q)**, aligned parallel to the z-axis for both samples (Fig. 1). The EMD was then determined by a qualitative interpretation of the preferred orientation of the two samples, by comparing relative intensities of the diffraction peaks with those of the free powder.

X-ray QTA was performed on Sample B using a Huber 4-circles diffractometer and the INEL curved position sensitive detector, which spans a 120° range in 2θ, for the simultaneous acquisition of several pole figures [11]. These measurements

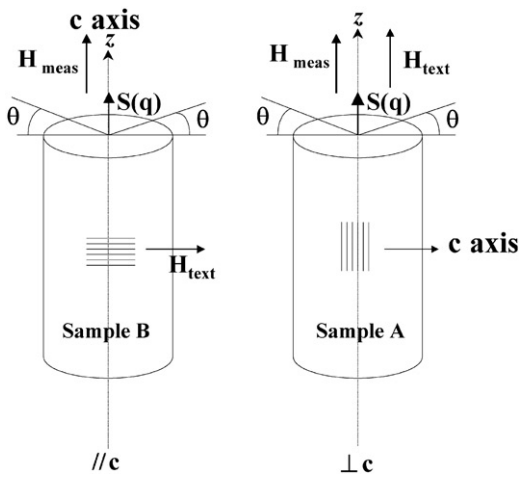

Fig. 1. Traditional technique (right column) and rotation alignment procedure (left column) used for the alignment of samples A and B, respectively. The geometry of X-ray diffraction measurements (**S(q)**) and the configurations for the magnetization measurements (H_{meas}) are also shown.

were made in order to determine the possibility to orient the magnetization axes under a relatively low magnetic field, and to determine the quantitative distribution of the c-axes used later in the anisotropic magnetization curve simulation.

Magnetization measurements were carried out on the free powder and on the aligned samples using an automated extraction magnetometer, in the 2–300 K temperature range. Measurements were performed for the oriented powders with an applied magnetic field, H_{meas}, parallel and perpendicular to H_{text} for Samples A and B, respectively (Fig. 1).

Neutron diffraction experiments were performed at $T = 300$ K on the $ErMn_4Fe_8C$ random powder using the D1B diffractometer ($\lambda = 2.522$ Å) of the ILL high-flux reactor in order to determine the microscopic magnetic properties.

3. Results and discussion

3.1. X-ray diffraction analysis

Classical X-ray diffraction diagrams recorded on the faces perpendicular to the z-axis of the samples and showing the {2 2 0} and {0 0 2} diffraction lines are presented in Fig. 2. The inset of this figure shows the full diffraction pattern of Sample B, which exhibits peak ratios different from those of a random powder, indicating the existence of a texture. However, all the lines are visible, revealing a relatively low texture strength. Looking at specific peaks, for instance those associated with the {2 2 0} and {0 0 2} families of planes, allows a first qualitative estimate of the texture. The patterns measured with **S(q)** parallel (Sample A) and perpendicular (Sample B) to H_{text} exhibit different {2 2 0}/{0 0 2} intensity ratios,

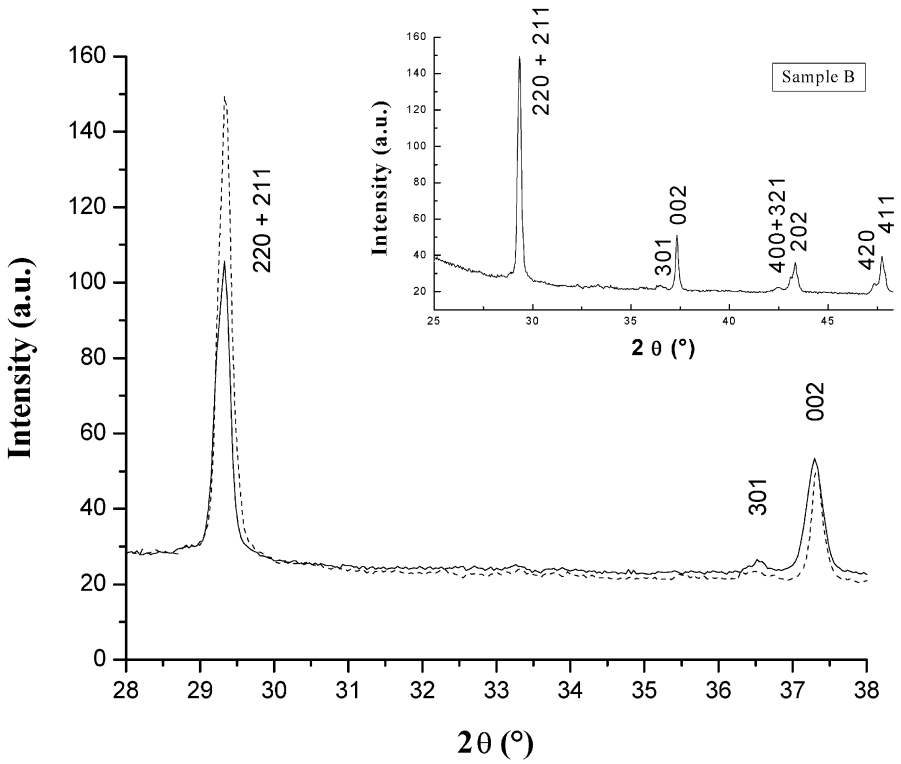

Fig. 2. X-ray diffraction pattern of the oriented $ErMn_4Fe_8C$ compound with H_{text} parallel (Sample A, dotted line) and perpendicular (Sample B, full line) to the cylinder axis. The inset shows the full diffraction pattern of Sample B.

with favored {2 2 0} reflections when H_{text} is applied parallel to **z** (Sample A), and favored {0 0 2} reflections for H_{text} perpendicular to **z**. This indicates that the mean EMD is located in the basal plane of the structure.

3.2. Quantitative texture analysis (QTA)

Quantitative texture analysis was performed on Sample B (oriented carbide with H_{text} perpendicular to the z-axis). We firstly verified that no significant change in the diffracted lines occurred when rotating the sample around the azimuth φ axis of the diffractometer, aligned parallel to **z**. Pole figures were then measured by scanning the tilt angle of the goniometer, χ, between 0° and 70° [11]. For the refinement of the orientation distribution function (ODF), we used the {3 2 1/4 0 0/2 0 2} and {4 2 0/4 1 1} groups of reflections, thus covering a large distribution of orientations. The experimental normalized pole figures (left column of Fig. 3(a)) determine the distribution of the normal to the $\{h\,k\,l\}$ planes, $\langle h\,k\,l\rangle$*. These pole figures are representative of a so-called "fibre texture", with crystalline axes randomly distributed around their normal (z-axis). The ODF refined using the Williams–Imhof–Matthies–Vinel (WIMV) method allows the recalculation of the experimental pole figures (Fig. 3(a), right column) [6]. A good reproduction of the experimental pole figures is obtained and this recalculation allows the completion of the blind and non-measured zones (appearing in white on the experimental pole figures) [11]. The average reliability factor [7] calculated on the {3 2 1/4 0 0/2 0 2} and {4 2 0/4 1 1} pole figures is only 1.2% and attests for the quality of the ODF refinement. Calculation of the low indices {0 0 1} and {1 0 0} pole figures allows a simpler texture visualization (Fig. 3(b)). The {0 0 1} planes are preferentially aligned perpendicular to the cylinder z-axis (normal of the figure plane) with a maximum orientation density about 3.9 times that of a random powder (measured in mrd units: multiple of a random distribution), showing a relatively low texture strength. A second orientation is observed with the {0 0 1} planes parallel to this axis (reinforcements observed around 1 mrd on the equator of the {0 0 1} pole figure). The minimum orientation density of 0.5 mrd indicates that 50% of the sample volume is randomly oriented.

From the point of view of the magnetic anisotropy, it is important to check if $\{h\,k\,l\}$ planes align with their normals along **z**, which would be difficult to evidence on the recalculated pole figures of Fig. 3(b). This can be directly checked by looking at the inverse pole figure calculated for the z-direction (Fig. 4). In this figure we have represented the Miller indices of the components having planes parallel to **z** and a maximum value larger than 1 mrd. One can retrieve the previously described {0 0 1} major and the {1 0 0} minor components, and also two other minor ones: {2 2 1} and {2 0 1}.

The texture strength is quantified with the texture index F^2 equal to 1.3 mrd^2. The degree of "texture disorder" is given by calculating the entropy S found to be equal to –0.13. The values of the F^2 and S indicate a relatively weak texture [4] but this orientation (4 times the free powder) would be sufficient to induce a large anisotropy of the magnetic behavior.

3.3. Magnetization measurements

In order to determine the magnetic properties associated with anisotropy, magnetization measurements $M(H)$ in the 2–300 K temperature range have been performed on the oriented $ErMn_4Fe_8C$ samples. The magnetic field used for these measurements, H_{meas}, was applied parallel and perpendicular to the c-axis for Samples B and A, respectively (Fig. 1) in order to determine the EMD. The notations $M_{\parallel}$ and $M_{\perp}$ correspond to the magnetization curves measured, respectively, on Sample B with $\mathbf{H_{meas}} \parallel \mathbf{z}$ (parallel to the mean **c**-axis direction) and on Sample A with $\mathbf{H_{meas}} \perp \mathbf{z}$ (perpendicular to the mean **c**-axis direction).

Whatever the temperature (Fig. 5), the EMD corresponds to the magnetization measurements performed on Sample B ($H_{meas} \perp H_{text}$), i.e. to the basal planes (**a**, **b**) of the structure, revealing the absence of spin reorientation transition (SRT) contrary to what was observed in the parent $RFe_{10.5}Mo_{1.5}X$ compounds ($X = H$, C) [12]. Differences are observed in the $M(H)$ curves between

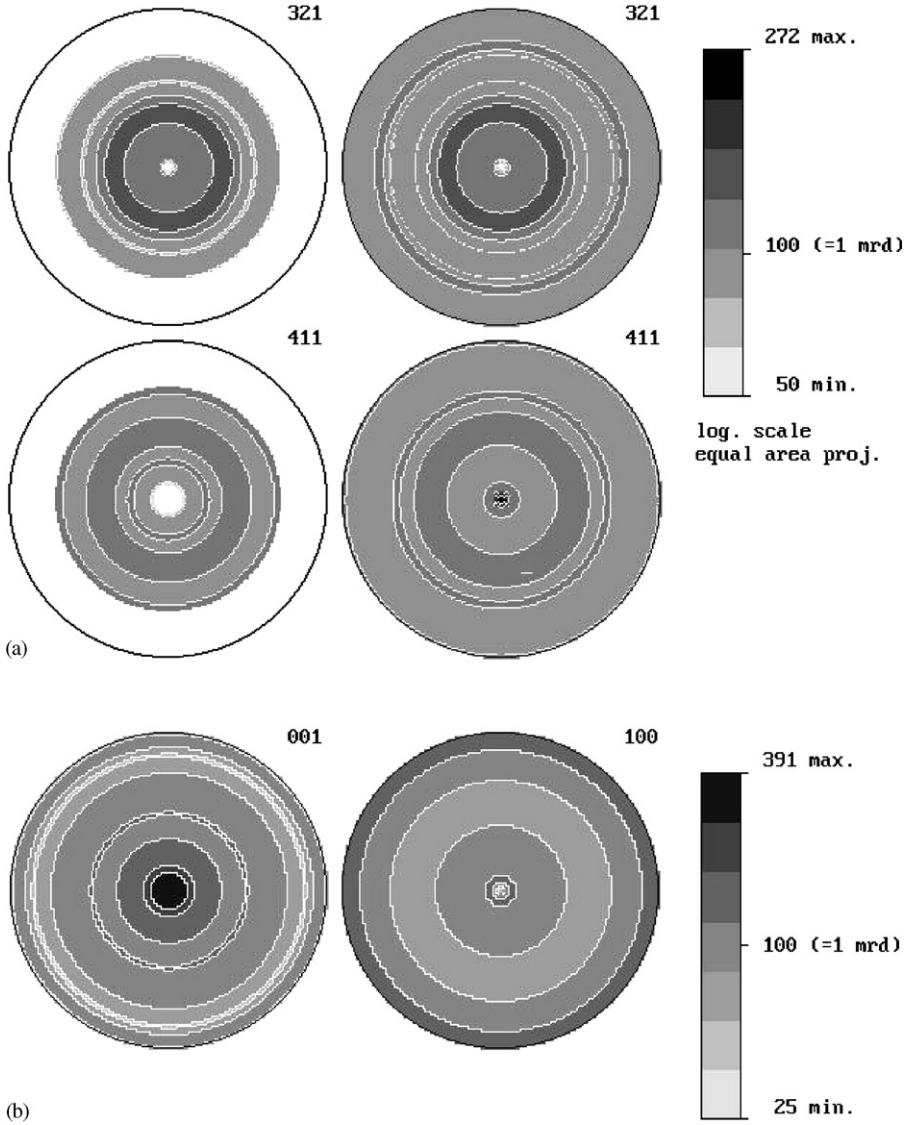

Fig. 3. (a) Experimental normalized {3 2 1/4 0 0/2 0 2} and {4 2 0/4 1 1} overlapped pole figures of Sample B (left column) and recalculated ones (right column) from the ODF. (b) Low-indices {0 0 1} and {1 0 0} recalculated pole figures. Logarithmic density scale, equal area projection.

the low and the room temperature ranges as seen in Fig. 5. From these curves, the anisotropy field H_A was determined as the junction point for which the applied field makes $M_{\parallel} = M_{\perp}$. Its thermal variation shows a maximum of 9 T close to 80 K (Fig. 6). In the RT_{12} structure type compounds, the magneto-crystalline anisotropy results from the competition between the rare-earth R and 3d(T) sublattices anisotropy. The latter dominates at high temperatures and could give rise to SRT if the former was dominating at low temperature, but it is not the case here [1]. Furthermore, it clearly appears that at lower temperatures (e.g. 4 K) the junction point is more complex than a

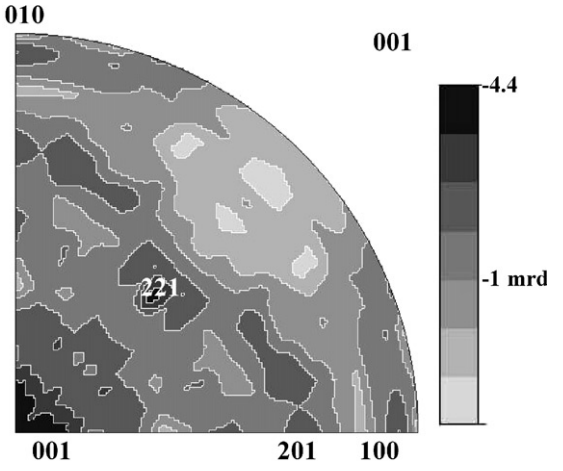

Fig. 4. Inverse pole figure calculated for the **z**-direction of Sample B, showing the low-density levels of the secondary components of the texture, significant of their low volume ratio. Logarithmic density scale, equal area projection.

simple anisotropy field H_A (Fig. 5), with the occurrence of a first-order magnetization process (FOMP) induced by the field, as already observed elsewhere in parent compounds [12,13,14].

The area in-between $M_{\parallel}$ and $M_{\perp}$ curves was used for a first estimate of the magneto-crystalline anisotropy energy W_A (Fig. 6). It markedly increases with temperature with a maximum close to 100 K and then exhibits a normal decrease going to $T_C = 370$ K. The relative difference observed at a temperature lower than 125 K between H_A and W_A should result from more complicated anisotropy contributions, e.g. from rare-earth crystal electrical field (CEF) with possibly higher order terms [14].

3.4. Neutron diffraction

Neutron diffraction experiments performed at 300 K on the free $ErMn_4Fe_8C$ powder allow the determination of the magnetic structure (Fig. 7) [2,3]. In agreement with the magnetization measurements and texture analysis, the collinear ferrimagnetic structure lies within the basal plane (**a**, **b**). This ferrimagnetic arrangement belongs to the E_g irreducible representation of the I4/mmm space group [2,3] and has been yet observed in the parent compounds $RFe_{12-x}Mo_xX$ (X = H, C, N) [11]. The antiferromagnetic coupling scheme between Er and the 3d sites of the $ThMn_{12}$ structure takes place in agreement with the Campbell theory for heavy rare-earth atoms [15]. Since the 8j and 8f sites are preferentially occupied by iron atoms, no ordered ferromagnetic moment was found at room temperature on the 8i sites (preferentially occupied by manganese atoms). The carbon atoms are located in the 2b site of the $ThMn_{12}$ structure type [2] in between the 2a positions of the Er atoms. The direct C–Er bonds strongly modify the CEF coefficients of the rare-earth atoms, which, in principle, give the largest contributions to the magneto-crystalline anisotropy [12,14]. This transformation from the easy-axis magnetic behavior of $ErMn_4Fe_8$ to the easy-plane magnetic behavior of $ErMn_4Fe_8C$ [2] fully agrees with the empirical rules determined for the parent $RFe_{12-x}Mo_xX$ (X = H, C, N) series [11]. Indeed, for the present case where the second-order Stevens factor α_J is positive [16], the C (or N) insertion markedly reduces the easy-axis character supported by the R atoms, and even transforms it into an easy-plane one [12]. The refined values of the ferromagnetic moments for each crystallographic site, determined using the general least-squares Material eXecutive Diffraction program (MXD) [17], are at $T = 300$ K (in μ_B/f.u.): $\mu_{8i} = 0$, $\mu_{8j} = -0.8(1)$, $\mu_{8f} = -1.3(1)$ and $\mu_{Er} = +1.7(1)$. They correspond to a reliability factor of 2.4% [17].

3.5. Numerical simulation of the $M(H)$ curves at $T = 300$ K

The magnetization $M(H_{meas})$ in an applied magnetic field H_{meas} can be expressed by

$$M(H_{meas}) = M_S \cos(\theta_0 - \theta), \quad (1)$$

where M_S is the saturation magnetization, θ is the angle between the c-axis of the crystal and the magnetization direction, and θ_0 the angle between H_{meas} and the c-axis of the crystallites (Fig. 8). At room temperature, the high-order anisotropy constants K_2, K_3, … are negligible in the $ThMn_{12}$ structure type compounds [13,14,18]. Although the exchange forces between the 3d(Mn, Fe) and Er sublattices are strong, the collinear magnetic arrangement of the $ErMn_4Fe_8C$ compound can

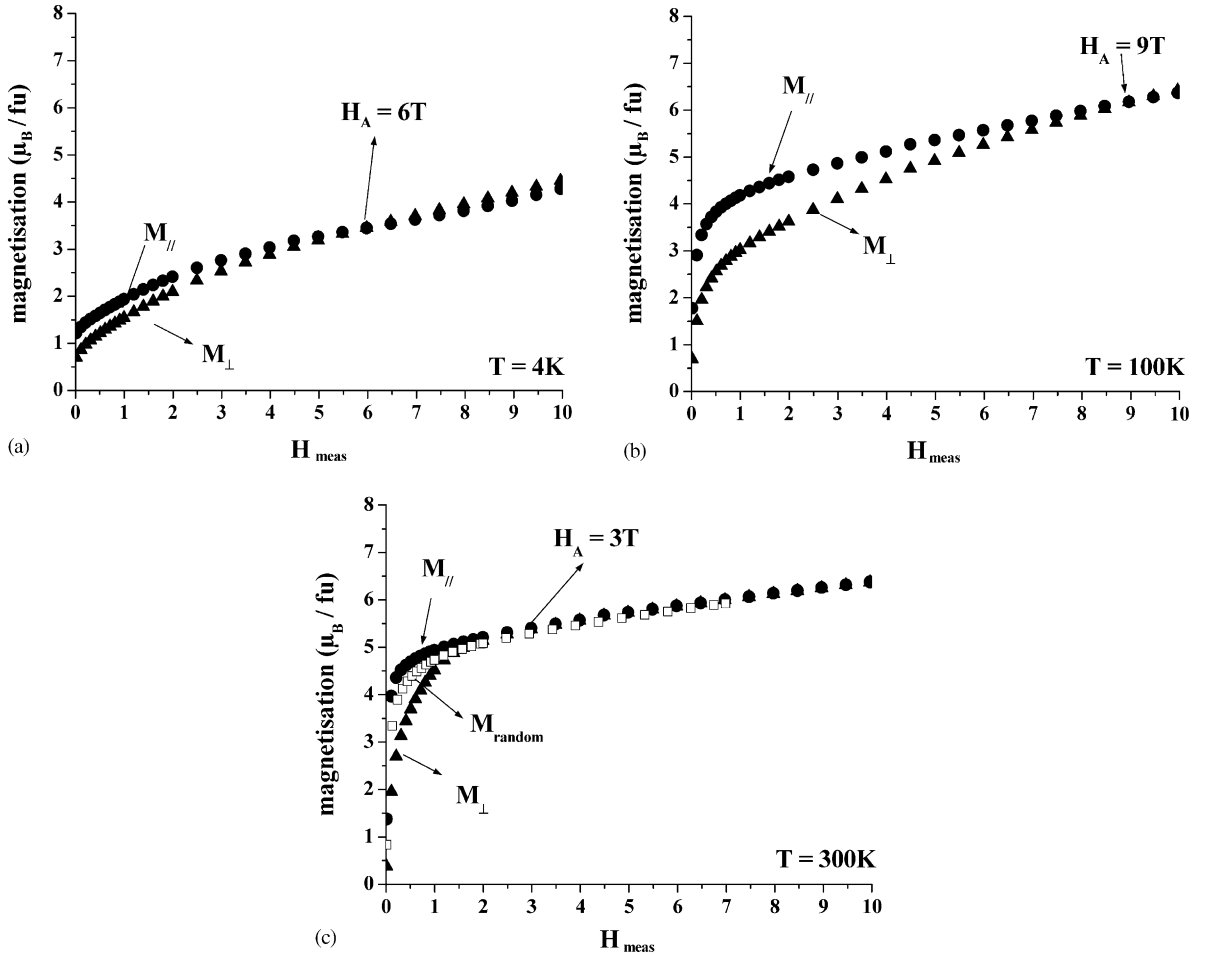

Fig. 5. Thermal behaviour of $M_{\parallel}$ (i.e. Sample B, $\mathbf{H_{meas}} \| \mathbf{c}$) and $M_{\perp}$ (i.e. Sample A, $\mathbf{H_{meas}} \perp \mathbf{c}$) magnetization curves of the $ErMn_4Fe_8C$ oriented compounds at (a) $T = 4\,K$, (b) $T = 100\,K$ and at (c) $T = 300\,K$. For $T = 300\,K$, the signal measured on the free powder M_{random} is also represented.

be considered as quasi-rigid for the H_{meas} not too large. Consequently, considering that the 3d and Er sublattices rotate in the same way with H_{meas}, the energy of the sample in an applied magnetic field can be expressed at $T = 300\,K$ by

$$E(H_{meas}) = K_1 \sin^2\theta - HM_S \cos(\theta_0 - \theta), \quad (2)$$

where K_1 is the first-order phenomenological anisotropy constant [14]. In this equation, the first term, $K_1 \sin^2\theta$, represents the anisotropy energy and the second, $-HM_S \cos(\theta_0 - \theta)$, the Zeeman energy. Here, this assumption appears relevant at high temperature only, since at low temperatures a more complex magnetic behavior occurs [2]. Under the equilibrium condition we have

$$\frac{dE}{d\theta} = 0 \quad (3)$$

which gives from Eq. (2)

$$H_{meas} = \frac{2K_1 \sin\theta \cos\theta}{M_S \sin(\theta_0 - \theta)}. \quad (4)$$

With an anisotropy field $H_A = 2K_1/M_S$ [14], the equilibrium condition becomes

$$\frac{H_{meas}}{H_A} = \frac{\sin\theta \cos\theta}{\sin(\theta_0 - \theta)}. \quad (5)$$

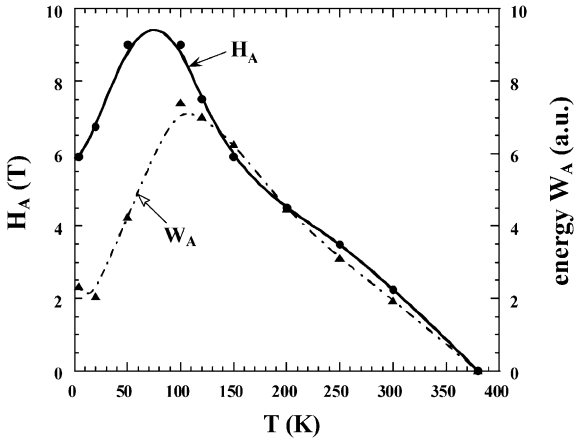

Fig. 6. Thermal behavior of the anisotropy field H_A (—) and magnetocrystalline anisotropy energy W_A ($\cdot$—$\cdot$) deduced from the anisotropic magnetization measurements.

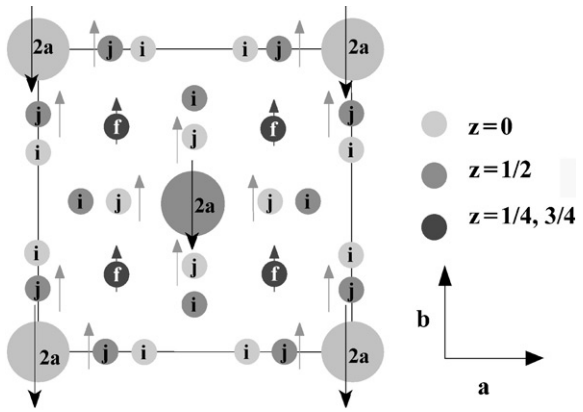

Fig. 7. Ferrimagnetic structure of the $ErMn_4Fe_8C$ in the basal plane (a, b) at $T = 300\,K$ deduced from neutron diffraction experiments.

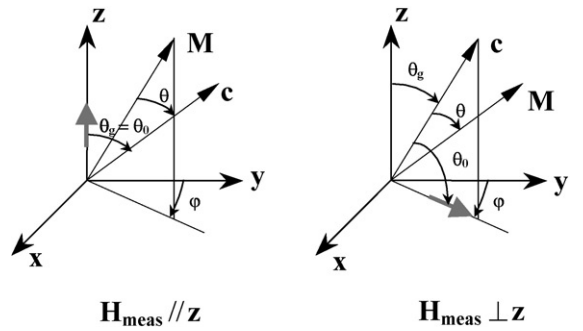

Fig. 8. The two configurations (a) $\mathbf{H}_{meas} \| \mathbf{c}$ and (b) $\mathbf{H}_{meas} \perp \mathbf{c}$ used for the measurement of the magnetization curves.

As magnetization curves in $ErMn_4Fe_8C$ are not saturated for a H_{meas} of 10 T, we evaluate the saturation magnetization M_S using a polynomial extrapolation [19]. Thus, under strong applied fields, there is no more domain wall displacement and the global magnetization variation is only due to the coherent rotation of the magnetic moments:

$$\frac{M}{H_{meas}} = \chi_0 - \frac{M_S}{H_{meas}} - \frac{AM_S}{H_{meas}^2} - \frac{BM_S}{H_{meas}^3}, \tag{6}$$

where χ_0 is the initial magnetic susceptibility and A and B are coefficients to be determined. The fit of $M_{\|}/H_{meas} = f(1/H)$ for the Sample B curve at $T = 300\,K$ gives $M_S = 6.37\,\mu_B$/f.u.

The studied sample can be represented by crystallites which have their crystallographic c-axes distributed uniformly around the z-axis, the texture direction [20]. The angular distribution of the magnetic moments, linked to the basal planes of the tetragonal structure, can be described by the probability function $F(\theta_g, \varphi)$ of finding the c-axis in a direction given by the θ_g and φ angles (Fig. 8). The θ_g angle measures the deviation of the c-axis from the z-axis (equivalent to the polar angle of the pole figures), and the angle φ refers to the projection of $\mathbf{c}$ in the (x, y) plane (azimuth of the pole figures). In fact the probability function is strongly correlated to the pole figures as measured by X-ray diffraction. Depending on the crystallite distribution function, a normalization procedure must be applied to the probability function $F(\theta_g, \varphi)$ [21]:

$$\int_{\theta_g=0}^{\pi/2} \int_{\phi=0}^{2\pi} F(\theta_g, \phi) \sin\theta_g \, d\theta_g \, d\phi = 1. \tag{7}$$

Considering that the $\mathbf{z}$-direction is a revolution axis of symmetry (axially symmetric texture), one can write $F(\theta_g, \varphi) = G(\theta_g) \times H(\varphi)$, where $H(\varphi)$ is a constant and $G(\theta_g)$ is the radial behavior of the textured volume distribution. Then the normalization condition (Eq. (7)) becomes

$$2\pi \int_{\theta_g=0}^{\pi/2} G(\theta_g) \sin\theta_g \, d\theta_g = 1. \tag{8}$$

For a random distribution (isotropic sample), $G(\theta_g)$ is a constant which is equal to $1/2\pi$. For a textured sample, this distribution reflects, to a certain extent, the crystallite distribution function,

if the magnetic moments are linked to specific crystal axes, as revealed by neutron diffraction for the $ErMn_4Fe_8C$ compound.

In Sample B, H_{meas} is parallel to the texturation direction **z**, which is perpendicular to the mean direction of the EMD. Then $\theta_g = \theta_0$ and the z-component of the magnetization is given by (Fig. 8):

$$M_z = \frac{M_\parallel}{M_S} = 2\pi \int_0^{\pi/2} G(\theta_g) \sin\theta_g \cos(\theta_g - \theta)\, d\theta_g, \quad (9)$$

where θ is calculated from Eq. (4) for every value of H_{meas} and θ_g.

The ODF refined from the texture experiments allows the calculation of the normalized pole figures $P_{\mathbf{h}}(\mathbf{y})$ which determine quantitatively the distribution of the directions $\langle h\,k\,l\rangle^*$ to the crystallographic planes $\{h\,k\,l\}$. The pole figure definition is given by [7]

$$\frac{dV}{V} = \frac{1}{4\pi} P_{\mathbf{h}}(\mathbf{y})\, d\mathbf{y} \quad (10)$$

with $\mathbf{h} = \langle hk\,l\rangle^*$, $\mathbf{y} = (\theta_g, \varphi)$ and $d\mathbf{y} = \sin\theta_g\, d\theta_g\, d\varphi$.

Here V is the irradiated volume of the sample and dV is the volume of crystallites having orientation between **y** and **y**+d**y**. The normalization condition for the pole figures is

$$\int_{\phi=0}^{2\pi} \int_{\theta_g=0}^{\pi/2} P_{\mathbf{h}}(\mathbf{y})\, d\mathbf{y} = 4\pi. \quad (11)$$

The radial {0 0 1} pole profile $G(\theta_g)$ determined by texture analysis is represented in Fig. 9. The variations observed at high θ_g angles are due to the existence of the minor components of texture described in the inverse pole figure (Fig. 4). From this figure, we estimate the total volume ratio associated with the three minor components to be no more than 5% in total. Since each of the minor component peaks at different θ_g values contribute with a low volume ratio to the magnetization, they can be interpreted by an average distribution. For a rotation-aligned sample, the {0 0 1} pole profile can be described by a Gaussian or a Lorentzian distribution about the z-axis [10]. The best fit of the {0 0 1} distribution (Fig. 9) was found for a Pseudo-Voigt (PV) shape of the distribution (mean

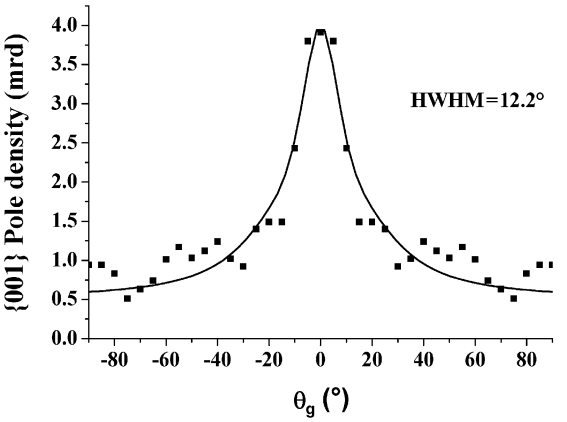

Fig. 9. PV fit of the {0 0 1} distribution density deduced from texture analysis. The randomly oriented background is 0.5 mrd, and the fit accounts for the main and the minor contributions.

weighted value of a Gaussian and Lorentzian distribution) with a half-width at half-maximum (HWHM) of 12.2° and a randomly distributed part of the volume, $\rho_0 = 0.5$ mrd (minimum of the distribution). From the definition of the pole figures, ρ_0 is directly the random volume ratio. Then, the contribution of the random part to the magnetization is the classical random magnetic signal, M_{random}, measured on free powder, times the volume ratio associated with this random component. So, the contribution to the magnetization of the textured part is in our case:

$$G(\theta_g) = (1 - \rho_0)\, PV(\theta_g). \quad (12)$$

Then Eq. (9) becomes

$$M_z = \frac{M_\parallel}{M_S} = 2\pi \int_0^{\pi/2} (1 - \rho_0)\, PV(\theta_g) \sin\theta_g \cos(\theta_g - \theta)\, d\theta_g + \rho_0 \frac{M_{random}}{M_S} \quad (13)$$

or finally

$$M_z = \frac{M_\parallel}{M_S} = 0.5 \frac{M_{random}}{M_S} + 0.5 \times 2\pi \int_0^{\pi/2} PV(\theta_g) \sin\theta_g \cos(\theta_g - \theta)\, d\theta_g. \quad (14)$$

Using this formalism, we have simulated the experimental magnetic curves $M_{\parallel}/M_S$ at $T = 300$ K. The fit of the $M_{\parallel}/M_S$ curves is shown in Fig. 10(a). A good reproduction of the experimental curve is obtained for low values of H_{meas}/H_A ratio (i.e. $H_{meas} < 1.8$ T) as shown in Fig. 10(b). This model does not take into account the rotation of the various magnetic moments for higher applied magnetic fields, which tend progressively to be aligned along the applied magnetic field.

The most important feature of the present approach is that the angular distribution of the moments is accounted for as a measured parameter. A fit of the anisotropic magnetization curves could be done (with an unknown distribution used to fit the same distribution shape), by using three more parameters in the fit (ρ_0, half-width, Gaussian to Lorentzian ratio). In such a case, it seems difficult to dissociate the texture from the magnetic effects, because the system becomes strongly under-determined, and the fitting procedure leads to unphysical parameters. However, using the present methodology, the texture effect is independently well identified, and the difference between measured and simulated magnetization curves can be associated with pure magnetic effects only.

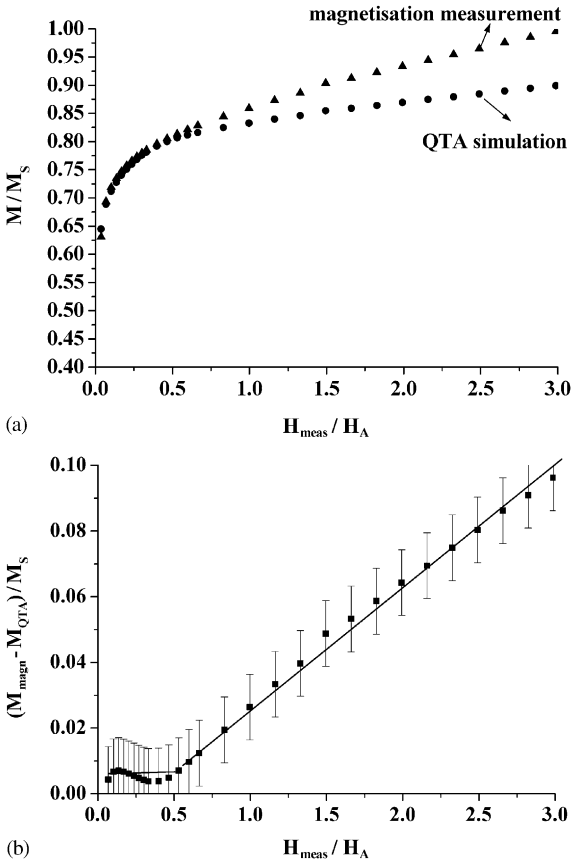

Fig. 10. (a) Comparison for Sample B of measured $M_{\parallel}/M_S$ ratio and simulated ($M_{texture}/M_S$) one and their difference (b). The line fit is only a guide for the eye and the constant error bars for this difference have been estimated to 0.01 to take into account the errors introduced by the instrument characteristics.

Also, because the texture is relatively weak, any peculiar shape of the second or higher-order derivative of magnetization versus magnetic field cannot be revealed [9]. The authors of Ref. [9] conclude that it is impossible to measure low texture using magnetization curves, particularly in the case of easy-plane materials. This means that the magnetization curves cannot determine complex textures, as that measured in the present work. Similarly, the methods developed by Searle et al. and Elk and Hermann [21,22] represent clear quantitative determination of the magnetic texture. However, these methods do not apply for complex textures since only one parameter (α_n in the original works) represents more than two characteristic features of the distributions, e.g. the half-width and the random background ρ_0. In our analysis, the random texture background deduced from a quantitative texture analysis was effectively subtracted. If not, attributing only one parameter to the texture effect yields an unrealistic overestimation of its amplitude [23].

Furthermore, another aspect of the QTA analysis should be mentioned. The way used to refine the ODF can introduce uncontrolled artifacts. Some authors [5] tried to make use of the generalized harmonic formalism in order to fit magnetization curves. It has been shown long ago that this formalism intrinsically underdetermines the ODF, creates non-physical negative density values (regrouped as "ghost phenomena"), and are not correctable in a physically understandable way [24]. Again in this case any magnetic effect in the magnetization curves is at least partially masked.

On the contrary, the WIMV approach corrects for the ghosts intrinsically.

3.6. Contribution to the magneto-crystalline analysis

The $ErMn_4Fe_8C$ compound exhibits an unusual magnetic structure supported by a rather complicated magneto-crystalline anisotropic behavior. In order to better understand the role of the different contributions to the magneto-crystalline anisotropy, high magnetic field measurements have to be undertaken, in particular at low temperature, where the erbium CEF terms are maximized. However, the present crystal analysis of a textured sample (under 0.5 T) reveals that even at 300 K, under the assumption of a simple expression for the magneto-crystalline energy ($W = K_1 \sin^2\theta$, Eq. (2)), a FOMP takes place under an applied magnetic field of about 1.8 T as seen in Fig. 10 (b). A direct analysis of the magnetization curves recorded at room temperature ($M_{\parallel}$ and M_S) cannot provide such a clear-cut result. Due to the low value of the magnetic field used to install the texture, even if the latter is far from complete, this texture was developed without any significant modification of the fundamental state of the magnetic structure (zero field state). The FOMP results from the application of a magnetic field out of the easy plane of magnetization [14]. The corresponding torque created on the different sublattices (R, 3d) is far more efficient to induce relative spin reorientation, than when the field is applied parallel to the easy plane. This reveals highly competing contributions between both the magneto-crystalline anisotropy terms and within the different exchange forces acting between the different sublattices. The antagonist parameters to be considered are not only acting between the global 3d terms on one side and the 4f terms on the other side. Furthermore, competitions between terms relative to the iron-rich and manganese-rich sites must be accounted. Note that in the $RMn_{12-x}Fe_x$ series, a planar non-collinear antiferromagnetic structure, rather weak 3d moments and exchange forces characterize the manganese-rich side whereas an easy c-axis ferromagnetic structure, larger 3d moments and higher exchange forces characterize the iron-rich side [25]. Recent X-ray magnetic circular dichroïsm (XMCD) analyses of the 3d element absorption edges allow us to assert local atomic pictures of the Fe and Mn magnetism [26]. A drastic weakening of the axial character of the erbium CEF terms in the RT_{12} series is realized by insertion of C atoms as first neighbors along the fourfold axis of the structure, once again superimposing a balance effect in the magneto-crystalline anisotropy energy [27,28].

4. Conclusion

This texture analysis performed at 300 K on samples aligned under a moderate field of 0.5 T allows us:

- to confirm that the $ErMn_4Fe_8C$ carbide is easy plane accordingly with neutron diffraction analysis;
- to simulate the magnetization curve versus field under the assumption of a simple expression to describe the magneto-crystalline anisotropy;
- to evidence a first-order magnetization process ($T = 300$ K, $H \approx 1.8$ T) that should result in the competition between different contributions to the magneto-crystalline anisotropy energy.

To our knowledge, it is the first time that an experimental determination of the texture is taken into account for the magnetization curve calculation of an easy-plane ferrimagnetic structure. The formalism developed here can be extended to any other texture type, even those exhibiting several texture components. In order to complete the magneto-crystalline anisotropy analysis, the texture measurements must be extended at low temperatures using both X-ray (crystallographic texture) and neutron (magnetic texture) techniques. This will enable us to account for higher anisotropy constants ($K_2, \ldots$) that have been neglected here reasonably in Eq. (2). These terms must be considered for a better description of the FOMP which are enhanced in carbides in comparison to the parent compounds RT_{12} [28].

References

[1] D. Fruchart, J.L. Soubeyroux, O. Isnard, S. Miraglia, E. Tomey, J. Alloys Compounds 219 (1995) 16.
[2] M. Morales, M. Bacmann, D. Fruchart, P. Wolfers, J. Magn. Magn. Mater. 236 (2001) 83.
[3] M. Morales, M. Bacmann, P. Wolfers, D. Fruchart, B. Ouladdiaf, Phys. Rev. B 64 (2001) 144426.
[4] B.A. Legrand, D. Chateigner, R. Perrier de la Bathie, R. Tournier, J. Magn. Magn. Mater. 173 (1997) 20.
[5] T. Walker, S. Wirth, D. Schläfer, N. Mattern, K.-H. Müller, A. Handstein, Mikrochim. Acta 125 (1997) 355.
[6] S. Matthies, G.W. Vinel, Phys. Stat. Sol. B 112 (1982) K111.
[7] H.-R. Wenk, S. Matthies, J. Donovan, D. Chateigner, J. Appl. Crystallogr. 31 (1998) 262.
[8] M. Morales, M. Bacmann, D. Fruchart, P. Wolfers, J. Magn. Magn. Mater. 196–197 (1999) 703.
[9] R. Vert, M. Bououdina, D. Fruchart, D. Gignoux, J. Alloys Compounds 287 (1999) 38.
[10] W. Qun, Z. Zhi-gang, L. Wei, X.K. Sun, Y.C. Chuang, J. Magn. Magn. Mater. 109 (1992) 59.
[11] H. Pillière, D. Chateigner, Program INEL/LPEC, 1999.
[12] E. Tomey, M. Bacmann, D. Fruchart, D. Gignoux, J.L. Soubeyroux, J. Alloys Compounds 262–263 (1997) 194.
[13] R. Vert, Ph.D. Thesis, Université J. Fourier, Grenoble, France, 1999.
[14] H.S. Li, J.M.D. Coey, in: K.H.J. Buschow (Ed.), Handbook of Magnetic Materials, Vol. 6, North-Holland, Amsterdam, 1991, pp. 1–83.
[15] J.A. Campbell, J. Phys. F: Met. Phys. 2 (1972) L47.
[16] N.T. Hutching, Solid State Phys. 16 (1964) 227.
[17] P. Wolfers, J. Appl. Crystallogr. 23 (1990) 554.
[18] B.P. Hu, H.S. Li, J.M.D. Coey, J. Phys.: Condens. Matter 1 (1989) 755.
[19] P. Weiss, R. Forrer, Ann. Phys. 12 (1929) 279.
[20] P. Tenaud, Ph.D. Thesis, Université J. Fourier, Grenoble, France, 1988.
[21] C.W. Searle, V. Davis, R.D. Hutchens, J. Appl. Phys. 53 (1982) 2395.
[22] K. Elk, R. Hermann, J. Magn. Magn. Mater. 138 (1993) 138.
[23] A. Yan, W. Zhang, H.-W. Zhang, B. Shen, J. Magn. Magn. Mater. 210 (2000) L10.
[24] S. Matthies, Phys. Stat. Sol. B 92 (1979) 135.
[25] M. Morales, Ph.D. Thesis, Université J. Fourier, Grenoble, France, 1999.
[26] M. Morales, M. Bacmann, D. Fruchart, P. Wolfers, Ch. Baudelet, A. Delobbe, G. Krill, J. Alloys Compounds 317 (2001) 470.
[27] D.P.F. Hurley, J.M.D. Coey, J. Phys.: Condens. Matter 4 (1992) 5573.
[28] H. Fujii, H. Sun, in: K.H.J. Buschow (Ed.), Handbook of Magnetic Materials, Vol. 9, North-Holland, Amsterdam, 1991, pp. 356–363.